BIOINFORMATICS ORIGINAL PAPER Vol. 28 no. 16 2012, pages 2146–2153
doi:10.1093/bioinformatics/bts354

Systems biology Advance Access publication June 23, 2012

Identification of feedback loops in neural networks based on multi-step Granger causality

Chao-Yi Dong[1], Dongkwan Shin[2], Sunghoon Joo[2], YoonKey Nam[2] and Kwang-Hyun Cho[2,*]

[1]Department of Automatic Control, Inner Mongolia University of Technology, Huhhot 010080, People's Republic of China and [2]Department of Bio and Brain Engineering, Korea Advanced Institute of Science and Technology (KAIST), Daejeon 305-701, Republic of Korea

Associate Editor: Olga Troyanskaya

ABSTRACT

Motivation: Feedback circuits are crucial network motifs, ubiquitously found in many intra- and inter-cellular regulatory networks, and also act as basic building blocks for inducing synchronized bursting behaviors in neural network dynamics. Therefore, the system-level identification of feedback circuits using time-series measurements is critical to understand the underlying regulatory mechanism of synchronized bursting behaviors.

Results: Multi-Step Granger Causality Method (MSGCM) was developed to identify feedback loops embedded in biological networks using time-series experimental measurements. Based on multivariate time-series analysis, MSGCM used a modified Wald test to infer the existence of multi-step Granger causality between a pair of network nodes. A significant bi-directional multi-step Granger causality between two nodes indicated the existence of a feedback loop. This new identification method resolved the drawback of the previous non-causal impulse response component method which was only applicable to networks containing no co-regulatory forward path. MSGCM also significantly improved the ratio of correct identification of feedback loops. In this study, the MSGCM was testified using synthetic pulsed neural network models and also *in vitro* cultured rat neural networks using multi-electrode array. As a result, we found a large number of feedback loops in the *in vitro* cultured neural networks with apparent synchronized oscillation, indicating a close relationship between synchronized oscillatory bursting behavior and underlying feedback loops. The MSGCM is an efficient method to investigate feedback loops embedded in *in vitro* cultured neural networks. The identified feedback loop motifs are considered as an important design principle responsible for the synchronized bursting behavior in neural networks.

Contact: ckh@kaist.ac.kr

Availability: The software implementing MSGCM is available at Supplementary Information.

Supplementary Information: Supplementary material are available at *Bioinformatics* online.

Received on October 28, 2011; revised on April 23, 2012; accepted on June 4, 2012

1 INTRODUCTION

Feedback circuits are key regulatory motifs in many biological systems. Previous studies show that positive feedback loops determine a variety of cellular processes such as development, cell proliferation, apoptosis and responses to stress (Eisen *et al*., 1967; Wolpert and Lewis, 1975), and negative feedback loops contribute to maintaining the homeostasis of biological systems under internal and external interferences (Kim *et al*., 2008; Maeda *et al*., 2004). Moreover, many functional modules in biological systems are composed of multiple feedback loops. Various nonlinear dynamic behaviors of biological systems are generated by combination of positive and negative feedback loops (Glendinning, 1994; Strogatz, 2000). Interlinked fast and slow positive feedback loops (Brandman *et al*., 2005) can form a 'dual-time' switch which is rapidly inducible and also resistant to noises propagated from the upstream signaling system. Coupled direct and indirect positive feedback loops induce robust synchronized bursting behaviors (Dong *et al*., 2009a).

Identifying the existence of an intra- or inter-cellular feedback circuit in biological networks is an important systems biological issue. A variety of network motif search tools (Alon, 2007) such as mfinder (Kashtan *et al*., 2002), FANMOD (Wernicke and Rasche, 2006) and MAVisto (Schreiber and Schwobbermeyer, 2005) were proposed to find small vertex-induced subgraphs (occurring more frequently than those in random networks) from a network with known topology, but such methods cannot be used to identify hidden feedback loops in a network with unknown topology from time-series measurements On the other hand, time-series measurements of dynamical responses are now increasingly available [e.g. real-time polymerase chain reaction (PCR) (Heid *et al*., 1996), microarray (Schena *et al*., 1995), immunofluorescence (Henle and Henle, 1966) and multi-electrode array (Chong *et al*., 2011)] and various types of biological networks can be investigated using such data. So, there is a pressing need to develop an efficient method to identify feedback loops from multi-channel dynamical response data. Based on time-series analysis and system identification theory, several methods have been proposed to tackle this problem. For instance, Caines and Chan (1975) proposed the likelihood ratio test method (LRTM) based on the minimum phase spectral factor (MPSF) which is a canonical representation of the power spectral density matrix of the joint stochastic process of input and output data. In LRTM, the feedback effect between two-partitioned node sets was investigated with *a priori* knowledge on the system order and structure. Although LRTM can identify a feedback loop between two-partitioned node sets, it cannot identify a feedback loop between two individual nodes in the network. Schnider *et al*. (1989) developed a direct coherence method in the frequency domain to detect feedbacks in the central

*To whom correspondence should be addressed.

nervous system. Subsequent studies have further developed and extended this method for other physiological applications such as detecting bi-directional hippocampal interactions between the CA3 and CA1 regions (Baccala and Sameshima, 1999) and quantifying the linear causal strength in closely interacting cardiovascular variability signals (Porta *et al*., 2002). The direct coherence approach can unravel the existence of a strong or weak feedback interaction between two variates, but a statistical test of this approach has not yet been provided. In our previous study, we have developed the non-causal impulse response component method (NIRCM) (Dong *et al*., 2009a, b) on the basis of correlation identification and spectral factor analysis. NIRCM does not require any explicit knowledge about the system order or structure and has also relatively low computational complexity, but it was only applicable to networks that do not include co-regulatory forward paths.

Although several different methods for identification of biological feedback loops have been developed, all the methods still have fundamental limitations in finding feedback interactions between individual nodes in complex biological networks without *a priori* knowledge on the system. Hence, it is indispensable to develop a more efficient identification method which can overcome such difficulties of the previous methods. In this study, we proposed a multi-step Granger causality method (MSGCM) to identify the feedback loops embedded in biological networks where a pair of nodes might share some common predecessors. Note that NIRCM cannot be applied to networks in case input and output noises from a pair of nodes are correlated through a co-regulating predecessor (Caines and Chan, 1975). Basically, MSGCM is a multiple time-series analysis method based on the vector autoregressive (VAR) model. So, it is suitable to identify feedback loops between any pair of network nodes by simultaneously analyzing all dynamical couplings inside the network. The parameter values of the VAR model are estimated using the multivariate least-squares method (MLSM) (Ruppert and Wand, 1994). Then, a multi-step causality test is applied to the VAR model with the estimated parameter values to infer the h-step causality between all pairs of nodes. In particular, modified Wald statistics were used to avoid the problem of matrix rank reduction (Lütkepohl, 2005). Finally, an asymptotic distribution of the Wald statistics was formed to examine the existence of h-step causality. Bi-directional h-step causality between a pair of nodes indicates the existence of a feedback loop between the two nodes. This method can be considered as a natural extension of the NIRCM to multivariate systems by introducing multivariate time-series analysis. Since the dynamical couplings between nodes can be decoupled by MSGCM, it will be more useful for the identification of feedback loops in a densely connected biological network. We applied the proposed MSGCM to synthetic neural network simulation data based on Spike Response Model (SRM) and also to the time-series data obtained from *in vitro* cultured neural networks. As a result, a significant number of feedback loops were identified from the synchronized oscillatory behaviors, indicating a close correlation between such behaviors and the underlying feedback loops.

2 METHODS

2.1 VAR model

Dynamical characteristics of complex systems such as biological networks can be inferred from the analysis of a multivariate stochastic model fitted to the observation of time-series data (Tiao and Box, 1981). In practice, many spontaneous time-series data are considered as the measured output of stationary stochastic processes (Ross, 1996). Assume $X_k = (x_1(k), x_2(k), \dots, x_N(k))'$ ($k = 0, \pm1, \pm2, \dots$, which indicates the time index) to be a stationary multivariate stochastic process. X_k denotes the N-dimensional measurements vector of the biological network composed of N-nodes. The purpose of feedback loop identification is to infer the bi-directional dynamical coupling between any pair of nodes $x_i(k)$ and $x_j(k)$, where $i,j = 1,2,\dots,N$ with $i \neq j$. In this study, the dynamical coupling is conceptually identical to the directional multi-step (say h-step, where h can be any positive integer up to infinity) Granger causality that is described in detail in the following section. If bi-directional multi-step Granger causalities are identified between two nodes, it means that a feedback loop exists between them.

Among various models representing stationary multivariate time-series data (Brillinger, 2001; Cadotte *et al*., 2008; Lütkepohl, 2005), the VAR model is selected here to model biological multivariate data because of its feasibility and ease of computations. The pth-order VAR model (VAR(p)) is constructed by expressing X_k, the value of a (multivariate) process X at current time k, with its past values weighted with certain coefficients A_l and a (multivariate) white noise value E_k:

$$X_k = V + \sum_{l=1}^{p} A_l X_{k-l} + E_k, \quad k = 0, \pm1, \pm2, \dots, \tag{1}$$

where $X_k = \left(x_1(k),\ x_2(k), \dots, x_N(k)\right)'$, $E_k = \left(e_1(k), e_2(k), \dots, e_N(k)\right)'$ and $V = \left(v_1, v_2, \dots, v_N\right)'$ which is a constant vector of intercept terms representing the mean of X_k.

For a given vector of multivariate time series, its VAR(p) model can be readily estimated by MLSM (Ruppert and Wand, 1994). Suppose that we have a sample of size L for each of N variates with the same sample period. The estimation of $A := \left[A_1,\ A_2,\ \dots\ , A_p\right]_{N \times Np}$ is calculated as follows:

$$\hat{A} = Y^0 X' \left(XX'\right)^{-1}, \tag{2}$$

where $Y^0 := [X_1 - \mu,\ X_2 - \mu, \dots, X_L - \mu]_{N \times L}$, $Y_k^0 := \begin{bmatrix} X_k - \mu \\ \vdots \\ X_{k-p+1} - \mu \end{bmatrix}_{Np \times 1}$,

$X := \left[Y_0^0,\ Y_1^0, \dots, Y_{L-1}^0\right]_{Np \times L}$ and $\mu := E(X_k) \approx \frac{1}{L} \sum_{k=1}^{L} X_k$.

In addition, an unbiased estimate of the covariance matrix Σ_E of E_k is obtained as (Lütkepohl, 2005)

$$\hat{\Sigma}_E = \frac{1}{L - Np - 1} \sum_{k=1}^{L} \hat{E}_k \hat{E}_k' = \frac{1}{L - Np - 1} (Y^0 - \hat{A}X)(Y^0 - \hat{A}X)'. \tag{3}$$

If the preceding estimation procedures are repeated for different p-values, the order of the VAR(p) model can be selected by HQ criterion (Hannan and Quinn, 1979) which provides an optimal solution of p using the knowledge of data size L, network dimension N and estimated covariance matrix $\hat{\Sigma}_E$. According to the HQ criterion, model order p is estimated by optimizing

$$\mathrm{HQ}(p) = \ln \left| \hat{\Sigma}_E(p) \right| + \frac{2 \ln \ln L}{L} p N^2. \tag{4}$$

Therefore, the optimal order can be determined as $p_{\mathrm{opt}} = \arg\min_p (\mathrm{HQ}(p))$. The advantage of the HQ criterion is that p_{opt} is a consistent estimator $\hat{p}$ converging in probability to p, which is superior to other estimators using different criteria such as Akaike Information Criterion (AIC), Final Prediction Error (FPE) and Schwarz (SC) (Lütkepohl, 2005).

2.2 *h*-Step optimal prediction and multi-step causality

The concept of multi-step Granger causality is defined in light of an optimal prediction of the future value of one variate by using the current and past values of all network variates (Granger, 1969). If a contribution to the prediction comes from the variate itself, it is considered as a self-coupling;

otherwise, if a contribution comes from the other variates, it is called an alien coupling. Such predicted effects include not only most recent contributions but also very earlier contributions of all variates, depending on how much delayed couplings reach from the variates. We use h-step (h can be $1, 2, \ldots, \infty$, and it denotes the number of sampling periods) to quantify such 'multi-step' delayed coupling effects. In the following, some crucial inferences, such as h-step optimal prediction of a process and multi-step Granger causality between network variates, are immediately derived from the identified VAR(p).

For an N-dimensional stable VAR(p) process denoted by $X_k = (x_1(k), x_2(k), \ldots, x_N(k))'$, it was shown that the minimum mean square error (MSE) predictor for prediction horizon h at prediction origin k is the conditional expected value

$$E_k(X_{k+h}) := E(X_{k+h} | \{X_l | l \leqslant k\}), \tag{5}$$

which minimizes the MSE of X_{k+h} (Lütkepohl, 2005). Herein, the notation $\{X_l | l \leqslant k\}$ stands for all available information of X until time k. For a zero mean representation of the VAR(p) model, the optimal h-step predictor (in the sense of minimum MSE) of X_k at origin time k can be represented as

$$X_k(h) = J(I_{Np} + \widetilde{A} + \widetilde{A}^2 + \cdots + \widetilde{A}^{h-1})\widetilde{V} + J\widetilde{A}^h \widetilde{X}_k, \quad h \in \{1, 2, \ldots, \infty\}, \tag{6}$$

where $\widetilde{A} := \begin{bmatrix} A_1 & A_2 & \cdots & A_{p-1} & A_p \\ I_N & 0 & \cdots & 0 & 0 \\ 0 & I_N & \cdots & 0 & 0 \\ \vdots & \vdots & \ddots & \vdots & \vdots \\ 0 & 0 & \cdots & I_N & 0 \end{bmatrix}_{Np \times Np,}$ $\widetilde{X}_k := \begin{bmatrix} X_k \\ X_{k-1} \\ \vdots \\ X_{k-p+1} \end{bmatrix}_{Np \times 1,}$

$\widetilde{E}_k := \begin{bmatrix} E_k \\ 0 \\ \vdots \\ 0 \end{bmatrix}_{Np \times 1,}$ $\widetilde{V} := \begin{bmatrix} V \\ 0 \\ \vdots \\ 0 \end{bmatrix}_{Np \times 1}$ and $J := [I_N : 0 : \cdots : 0]_{N \times Np}$.

The h-step prediction error is $E_k(h) = X_{k+h} - X_k(h) = \sum_{m=0}^{h-1} \Phi_m e_{k+h-m}$ and the corresponding prediction error covariance matrix is $\Sigma_X(h) = \sum_{m=0}^{h-1} \Phi_m \Sigma_E \Phi_m'$, where $\Phi_m := J\widetilde{A}^m J'$ and Σ_E is the covariance matrix of white noises E_k. The proof of the above derivation is provided in the Supplementary Material (Section 1).

Equation (6) shows how all the network variates contribute to predicting each single variate. For instance, $x_j^k(h)$, which corresponds to the jth row in Equation (6) (j= 1, 2, … , N), is the optimal (minimum MSE) h-step predictor of the jth variate $x(k)$ at origin k obtained by using the current and past information of all variates. The corresponding prediction MSE is denoted by $\Sigma_{x_j}(h | \{X_l | l \leqslant k\})$ (i= 1, 2, … , N). The prediction MSE will increase if the information of some preceding variables is not considered. So, multi-step Granger causality from a stochastic variate $x_1(k)$ to another variate $x_2(k)$ was formally defined as follows (Granger, 1969): the process $x_1(k)$ is said to cause $x_2(k)$ in multi-step Granger's sense if

$$\Sigma_{x_2}(h | \{X_l | l \leqslant k\}) < \Sigma_{x_2}(h | \{X_l | l \leqslant k\} \setminus \{x_1(s) | s \leqslant k\}) \tag{7}$$

for at least one $h \in \{1, 2, \ldots, \infty\}$ (in practice, we only need to check for a finite step—see later of this section for details), i.e. the prediction of $x_2(k)$ can be improved if the past and current information in $x_1(k)$ is taken into account in addition to all the relevant information under consideration [the backslash in Equation (7) denotes the exclusion of the information of $\{x_1(s) | s \leqslant k\}$].

Note that the case of $h = 0$ is considered as instantaneous Granger causality which is physically unfeasible in biological networks because there is usually a significant time delay accompanied with the coupling process. So, we have excluded in this article such instantaneous Granger causality as well as self-coupling for nontrivial discussion. That is, only delayed alien (between different variates) couplings are considered in this article. Feedback loops are found when significant bi-directional multi-step Granger causalities are identified between two different network variates.

Multi-step Granger causality is fairly easy to evaluate in the context of a VAR model. Let us consider the multi-step Granger causality between two variates $x_i(k)$ and $x_j(k)$ ($i, j = 1, 2, \ldots, N$ and $i \neq j$) in an N-dimensional network. Consistent with the definition of multi-step Granger causality, $x_i(k)$ is called h-step non-causal for $x_j(k)$ if the m-step ahead predictions of $x_j(k)$ cannot be improved for all $m \leqslant h$ by taking into account the past and present $x_i(l)(l \leqslant k)$. Therefore, $x_i(k)$ is h-step non-causal for $x_j(k)$ if and only if all elements in the jth row and ith column in matrix $\left[J\widetilde{A}^h\right]_l$, which is the lth column block matrix of $J\widetilde{A}^m$ (for $m = 1, 2, \ldots, h$ and $l = 1, 2, \ldots, p$), are zeros. This means that there is no contribution from the regulating variate $x_i(k)$ to the prediction of the regulated variate $x_j(k)$ until h-step delays. We can derive this from h-step optimal predictor $X_k(h)$ [see Equation (6) and its expansion in Equation (8)]:

$$X_k(h) = J(I_{Np} + \widetilde{A} + \widetilde{A}^2 + \cdots + \widetilde{A}^{h-1})\widetilde{V} + \left[J\widetilde{A}^h\right]_1 X_k + \left[J\widetilde{A}^h\right]_2 X_{k-1} + \cdots \left[J\widetilde{A}^h\right]_p X_{k-p+1}. \tag{8}$$

For a two-partitioned process, one-step Granger causality is equivalent to multi-step Granger causality (details can be found from Baccala *et al*., 1998). The problem of feedback identification is now transformed into a problem of investigating whether non-diagonal blocks in A_l ($l = 1, 2, \ldots, p$) are zero simultaneously or not. However, in most biological networks, researchers are often interested in the causal couplings between a pair of variates rather than those between two-partitioned variate sets. Therefore, it is necessary to develop an approach to identify the multi-step Granger causality between any two variates in a higher dimensional network ($N \geqslant 3$). In the previous analysis, we need to prove h-step non-causality up to infinity to show that $x_i(k)$ does not contribute to the predictions of $x_j(k)$ (in the sense of multi-step Granger causality) in a multi-dimensional network. This task seems daunting and time-consuming. However, Dufour and Renault (1998) showed that we only need to examine a limited step of $p(N-2)+1$ instead of examining until infinite steps. This makes a statistical test of the MSGCM feasible for computation. See Supplementary Material (Section 2) for details on the modified Wald test to examine the multi-step Granger causality.

2.3 The algorithm for identification of feedback loops based on MSGCM

In this section, we propose an algorithm to identify feedback loops in multivariate biological networks. As this algorithm is based on the foregoing multi-step Granger causality test, it is called the MSGCM. The MSGCM algorithm can be implemented in Matlab 2007 (Mathworks, Inc.) [codes are provided in the Supplementary Material (Section 8)] and the identification steps are summarized in Figure 1.

The aforementioned algorithm can identify direct couplings as well as indirect couplings, i.e. when the signal from one node is or is not relayed through another node(s) before reaching the target node since the predictions for one variate would naturally include these two parts of contributions that usually appear in different prediction step h. In the following section, MSGCM is applied to simulated datasets obtained from computational neural network models [i.e. synthetic pulsed neural networks, see the Supplementary Material (Section 3) for a brief introduction of the models]. It turns out that MSGCM can successfully identify the direct as well as indirect feedback loops in two-, three- and (a more complicated) six-node networks. See the Supplementary Material (Section 4) for details on the sampling method of spike data. In our analysis, we used a limited bin size to low-pass filter the spike train data. In particular, a bin size of 10 ms was chosen to minimize false-positive identification (Golub and Van Loan, 1996). The sampling with a 10 ms interval corresponds to the low-pass filtering with the cutoff frequency of 100 Hz, which can filter out high frequency noises that contribute to false-positive identifications.

2.4 Multichannel recordings of *in vitro* neural networks

Hippocampal or cortical neurons used for developing *in vitro* neural networks were isolated from the brain of the Sprague-Dawley rat at embryonic day 18 (E18). Mechanically dissociated neurons were seeded on a planar-type microelectrode array (MEA) which has 60 surface-embedded

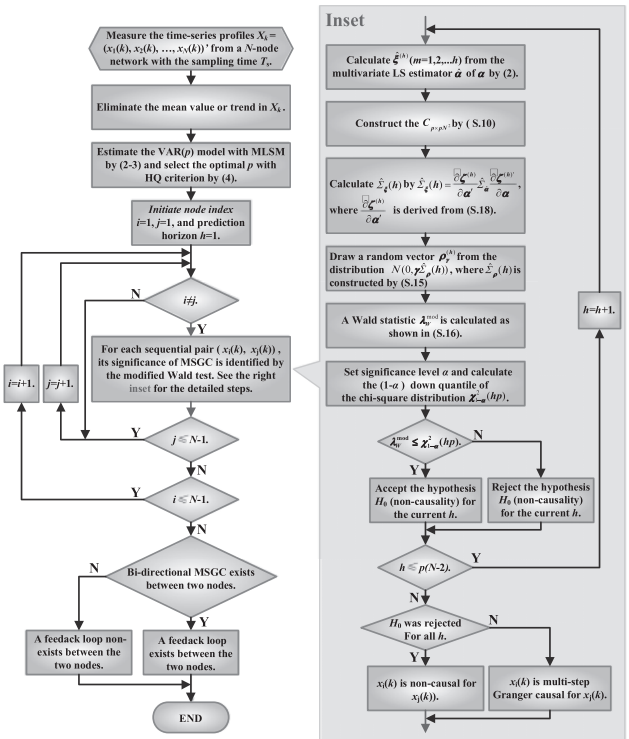

Fig. 1. The flow chart of the algorithm of MSGCM. The right inset shows the detailed sub-steps for identifying the significance of multi-step Granger causality for a sequential pair $(x_i(k),x_j(k))$ by the modified Wald test

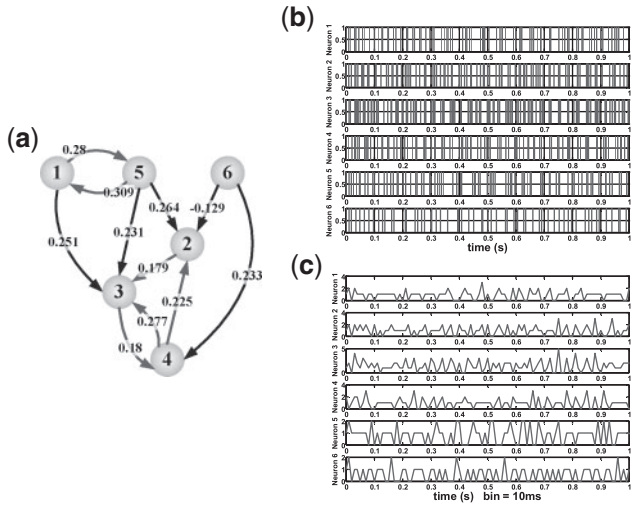

Fig. 2. A six-node pulsed neural network simulations. (**a**) The scheme of the six-node pulsed neural network. The red arrows highlight the locations of two direct feedback loops (1,5) and (3,4) and one indirect feedback loop (2,3,4). The weights of the synapses are denoted by the numbers around the arrows. (**b**) The raster plots of six neuron recordings (only the first 1 s segment of 20 s is shown). (**c**) The sampled time series from the six spike trains after binning them at 10 ms interval (only the first 1 s second segment of 20 s is shown)

microelectrodes for neural signal recordings. The MEA was cultivated in a humidified incubator with 37˚C, 5% CO_2. After 2 weeks of maturation period inside the incubator, the cultured MEA chip was connected with a MEA1060-BC preamplifier (Gain 50, BW 0.1—8500 Hz; Multi Channel Systems, Reutlingen, Germany) and FA60S amplifier (Gain 20, BW 10—5000 Hz; Multi Channel Systems). Multichannel signals were digitized and processed by MC Rack (Multi Channel Systems) and Offline Sorter (Plexon Inc., TX, USA). Extracellular action potentials (spikes) were detected by setting the threshold level at 5× standard deviation (SD of background noise level) and spike waveforms were classified (sorted) by principal component analysis (PCA) using dedicated spike sorting program (Offline Sorter). There can be multiple neurons (or units) generating spikes near a sensor. So, detected spikes are classified and clustered according to the shape of spikes. PCA has been used as one of the classification techniques to find a well-clustered spike signals (Hill *et al*., 2011).

3 RESULTS

3.1 Synthetic neural network simulations

To examine the efficacy of MSGCM for identification of feedback loops, we first applied it to two- and three-node pulsed neural networks of 12 different topologies as shown in Supplementary (Section 5) Figure S3a. The spike trains of each network were displayed for a period of 1 s, extracted from 20 s simulations [Supplementary (Section 5) Fig. S3b]. Finally, the sampled time-series data of the neurons in each network were obtained as shown in Supplementary (Section 5) Figure S3c. Based on these time-series data, MSGCM was applied to the six networks. As a result, we successfully identified the existence of feedback loops in all two- and three-node network topologies. The key parameters and results for identifications are summarized in Supplementary (Section 5) Table S1.

The MSGCM was also applied to a more complicated six-node network model containing two direct feedback loops and one indirect feedback loop. We constructed this model based on the same dynamical mechanism as those of the previous two- and three-node pulsed neural network models (Fig. 2a). Based on the obtained time-series data (Fig. 2c), MSGCM was then used to identify the existence of feedback loops with three multiples of the SD credence level ($\alpha = 0.00135$). Using HQ criterion, we determined an optimal order $p_{\text{opt}} = 6$ which corresponds to an HQ value of -7.5071. With the estimated parameters of the VAR(6) model, the Wald statistics showed significant Granger causalities in the network (Table 1). Since the bi-directional Granger causalities exist, we conclude that there is a feedback loop between neuron 1 and neuron 5. In the same way, we identified the other bi-directional couplings between neurons (2,3), (3,4) and (2,4). At this stage, we do not know whether the identified feedback loops are direct or indirect. However, MSGCM can correctly discern the existence of feedback loops between any pair of nodes. So, we can eventually identify all direct or indirect feedback loops.

3.2 Comparison of MSGCM and NIRCM

For quantitative comparison of the efficacies of MSGCM and NIRCM, we applied both methods to the same synthetic pulsed neural networks and compared their identification results. We simulated [with the same simulation protocol as detailed in the Supplementary Material (Section 5)] a number of neural networks of different sizes ranging from 6 to 20 nodes. Simulations were performed using SRMs for realization of randomly connected

Table 1. The identified multi-step Granger causalities in the six-node synthetic neural network

Node	1	2	3	4	5	6
1	0	0 (256.1 < 263.6)	0 (190.8 < 263.6)	0 (250.3 < 263.6)	1 (611.6 > 263.6)	0 (205.9 < 263.6)
2	1 (339.1 > 263.6)	0	1(331.9 > 263.6)	1 (424.2 > 263.6)	1 (578.1 > 263.6)	1 (308.5 > 263.6)
3	1 (402.2 > 263.6)	1 (286.0 > 263.6)	0	1 (523.3 > 263.6)	1 (472.0 > 263.6)	0 (222.7 < 263.6)
4	1 (314.4 > 263.6)	1 (301.6 > 263.6)	1 (451.6 > 263.6)	0	1 (325.2 > 263.6)	1 (335.3 > 263.6)
5	1 (474.9 > 263.6)	0 (225.3 < 263.6)	0 (212.7 < 263.6)	0 (189.2 < 263.6)	0	0 (231.3 < 263.6)
6	0 (183.2 < 263.6)	0 (183.3 < 263.6)	0 (215.9 < 263.6)	0 (219.3 < 263.6)	0 (185.0 < 263.6)	0

The '1's in the table represent the existence of significant Granger causalities from a column index to a row index, while '0's denote the non-existence of any significant Granger causality. The comparison between λ_W^{mod} and $\chi^2_{1-\alpha}(hp)$ is listed to the right of the identified results, where if $\lambda_W^{\mathrm{mod}} \le \chi^2_{1-\alpha}(hp)$, then '0' is inferred and if $\lambda_W^{\mathrm{mod}} \le \chi^2_{1-\alpha}(hp)$, then '1' is inferred. The four red-colored '1's in a symmetrical position by the right diagonal show the three identified feedback loops, which corresponds two pairs of bi-directional Granger causalities across nodes (1,5), nodes (3,4), nodes (2,3) and nodes (2,4).

Table 2. The means and standard deviations of the ratios of correct identifications, the false-positive ratios, and the false-negative ratios for different network scales with Connective Ratio (CR) of 20% and Excitatory Ratio (ER) of 90%

Network scale (the number of nodes)	Correct identification ratio		False-positive ratio		False-negative ratio	
	MSGCM	NIRCM	MSGCM	NIRCM	MSGCM	NIRCM
6	0.906 ± 0.105	0.781 ± 0.145	0.089 ±0.108	0.213 ± 0.150	0.006 ± 0.019	0.006 ± 0.019
8	0.968 ± 0.040	0.835 ± 0.121	0.014 ±0.034	0.164 ± 0.119	0.018 ± 0.022	0.001 ± 0.006
10	0.968 ± 0.026	0.843 ± 0.074	0.002 ±0.006	0.154 ± 0.073	0.031 ± 0.026	0.003 ± 0.008
12	0.959 ± 0.022	0.874 ± 0.059	0.000 ±0.000	0.123 ± 0.059	0.041 ± 0.022	0.003 ± 0.007
14	0.959 ± 0.018	0.879 ± 0.052	0.000 ±0.000	0.117 ± 0.052	0.041 ± 0.018	0.003 ± 0.006
16	0.961 ± 0.018	0.882 ± 0.043	0.000 ±0.000	0.113 ± 0.043	0.039 ± 0.018	0.006 ± 0.007
18	0.958 ± 0.017	0.871 ± 0.036	0.000 ±0.001	0.121 ± 0.035	0.042 ± 0.017	0.008 ± 0.007
20	0.958 ± 0.014	0.887 ± 0.034	0.000 ±0.001	0.103 ± 0.034	0.042 ± 0.014	0.010 ± 0.007

For each network scale, 100 randomly connected networks were tested using MSGCM and NIRCM.

networks where the synaptic efficacies w_{ij} were randomly chosen from a uniform distribution [−1, 1] [see Supplementary Material (Section 3) for further details on SRM]. For *in vitro* cultured neural networks, it has already been shown that each neuron is mono-synaptically connected to 10–30% of all other neurons at their matured phase and a matured inhibitory synaptic ratio of all the synapses is about 10–20% (Jimbo *et al.*, 1999; Marom and Shahaf, 2002). To mimic such *in vitro* cultured neural networks, the structure of the simulated network was randomly formed by keeping CR of 20% and ER of 90% [see detailed definitions of CR and ER in the Supplementary Material (Section 7)].

For each network size, 100 randomly connected networks were tested for identification of their feedback loops using the two methods. For each n-node network, we judged whether the feedback loop identification is correct or not with respect to all pairs of nodes. Then, for all the pairs of nodes ($n(n-1)/2$ in total), we counted the following four categorized cases: (1) the number of cases for correct identification of a feedback loop, n_{cf}; (2) the number of cases for correct identification of no feedback loop, n_{cnf}; (3) the number of cases for false-positive identification of a feedback loop, n_{fp} and (4) the number of cases for false-negative identification of no feedback loop, n_{fn}. Then, the ratio of correct identifications is defined as $2(n_{\mathrm{cf}}+n_{\mathrm{cnf}})/(n(n-1))$; the false-positive ratio as $2n_{\mathrm{fp}}/(n(n-1))$ and the false-negative ratio as $2n_{\mathrm{fn}}/(n(n-1))$. The means and SDs of the defined three ratios using two different methods were shown in Table 2.

The simulation results showed that the correct identification ratios of MSGCM are always significantly higher than those of NIRCM. Both methods had a low level of means for false-positive and false-negative ratios. The false-positive ratios of MSGCM were significantly less than those of NIRCM and the false-negative ratios of MSGCM were slightly higher than those of NIRCM.

3.3 Investigation of feedback loops in cultured neural networks

In previous sections, we showed the efficacy of MSGCM in identifying feedback loops in the artificial neuronal networks. Then, we also investigated the presence of feedback loops in real biological neural networks that spontaneously generate dynamical behaviors. The experimental data were obtained from a MEA (diameter 30 μm and spacing 200 μm) which can measure electrical signals (extracellular spikes) present in *in vitro* hippocampal neural networks (Eytan *et al.*, 2003, 2004; Marom and Shahaf, 2002; Shahaf and Marom, 2001). A detailed experimental protocol is described in the Supplementary Material (Section 6). Three 40 s segments of spike trains obtained from three independent cultures (Cultures 1–3 with the same experimental protocols) were used to testify the effectiveness of the proposed identification method. Only 9 out of total 60 channels had significant spike responses (the numbers of spikes are >10) in each culture. We excluded the channels showing insignificant data containing <10 spikes. As a result, some feedback loops were identified in the first three cultures, as shown in Table 3.

Table 3. The identification results of feedback loops in four cultured neural networks obtained by applying MSGCM and NIRCM

Network index	Age of network (DIV)	No. of nodes	Average BR (bursts/min)	Average SI (bin = 0.2 s)	No. of identified feedback loops by MSGCM	No. of identified feedback loops by NIRCM
1	14	9	9.2	0.6918	**11**	**20**
2	18	9	31.7	0.8707	**22**	**20**
3	21	9	7.3	0.3943	**4**	**6**
4	7	10	1.8	0.0033	**0**	**1**

The age of each sample network is defined by DIV (days *in vivo*). Average SIs were calculated by averaging the SIs for all possible channel pairs in each culture with a time bin of 0.2 s; average burst rates (BR) are the counted number of bursts happening in per minutes for all nine channel data.

Culture 4 was a micro-island neuronal culture in an agarose micro-well array (Kang *et al*., 2009) in which all physical connections between neurons were 'cut off' by the deliberate design. Then, electrodes under Culture 4 recorded spike trains from completely isolated neuronal circuits. Each electrode presented bursting activity generated by a few neurons, but the activity was not able to propagate through other electrodes due to the absence of biological connections between the electrodes. Therefore, the resultant spike trains of each electrode were affected by neurons from other electrodes. This was confirmed by applying MSGCM, as no feedback loop from Culture 4 was identified among 10 electrodes, as shown in Table 3. Therefore, the identification validated the feedback free cases in this non-connective culture. We also tried to identify feedback loops in the four cultures using NIRCM. The resulting identified feedback loops are shown in Table 3.

Although the number of channels was similar in all experiments, the identified feedback loops were different depending on the temporal patterns of spike trains. In particular, the enrichment of identified feedback loops was related to synchronized bursting behaviors. To quantify the temporal relationship of a pair of channels, the cross-correlation coefficient of the two binned data was defined as a synchrony index (SI) (Sasaki *et al*., 1989; Wylie *et al*., 1995). In this study, a sample correlation coefficient was calculated to approximate the cross-correlation coefficient. Given two binned data, $x(k)$ and $y(k)$ $(k=1,2,\ldots,L)$, then the sample correlation coefficient is as follows:

$$r_{xy}=\frac{\sum_{k=1}^{L}(x(k)-\bar{x})(y(k)-\bar{y})}{\sqrt{\sum_{k=1}^{L}(x(k)-\bar{x})^2\sum_{k=1}^{L}(y(k)-\bar{y})^2}}$$

where $\bar{x}=\frac{1}{L}\sum_{k=1}^{L}x(k)$ and $\bar{y}=\frac{1}{L}\sum_{k=1}^{L}y(k)$. Average SIs were then calculated by averaging the SIs for all possible pairs of channels in each culture to evaluate the degree of synchronized behaviors. In the raster plots of Cultures 1 and 2, we can find apparent synchronized oscillations among most of the electrodes (Fig. 3). This was also indicated by high SI index in Table 3. For Culture 3, SI index was significantly smaller than Cultures 1 and 2 despite high burst rates. These distinct behaviors were closely linked to the existence of a feedback loop. A larger number of feedback loops were found from Cultures 1 and 2 than Culture 3 (Table 3). As expected, Culture 4 did not show any synchrony due to the isolation of each electrode indicating no identified feedback loop from the spike trains in Culture 4.

Figure 4 shows two sets of feedback loops identified from Cultures 1 and 3, respectively. We can see a distinct distribution of feedback loops between these two cultures. Culture 1, presenting apparent synchronized oscillatory behavior, had 11 feedback loops among 9 electrodes, whereas Culture 3, showing less synchronized oscillations, had just 4 feedback loops.

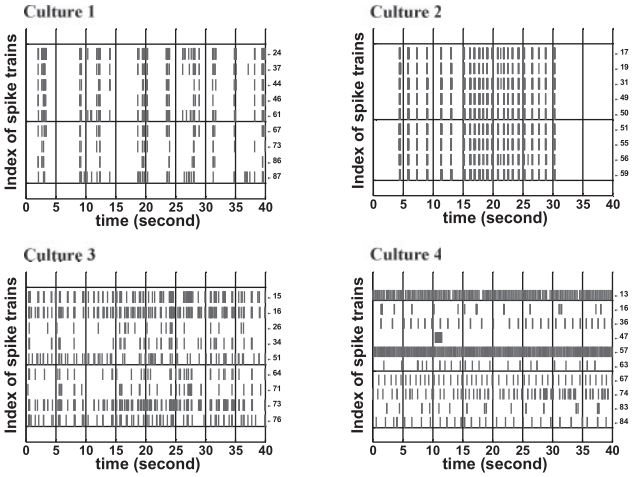

Fig. 3. The four 40 s segments of spike trains obtained from Cultures 1–4. Spike trains in Cultures 1–3 were from massively inter-connected neural networks, while spike trains in Culture 4 were from isolated micro-neural clusters by cell repulsive layer (agarose solution 2% wt/vol (mg/ml)). The numbers of identified feedback loops are summarized in Table 3

4 CONCLUSION

In this study, we investigated the problem of identifying feedback loops embedded in intra- or inter-cellular biological networks using time-series measurements. Based on multivariate time-series analysis, our proposed MSGCM can simultaneously analyze all network variates in the process of identifying the feedback loops from complicated biological networks. MSGCM can completely decouple the correlations between a pair of examined variates and the remaining variates in the network. This makes MSGCM overcome the shortcoming of NIRCM since co-regulatory forward paths always cause an input–output noise correlation. In this regard, MSGCM is more advanced than NIRCM and suitable for complex multivariate systems like biological networks. The application of MSGCM and NIRCM to the same synthetic pulsed neural networks showed that the correct identification ratios of MSGCM are always significantly higher than those of NIRCM. Although MSGCM can identify feedback loops of multivariate networks more accurately, its computational complexity is higher than NIRCM. However,

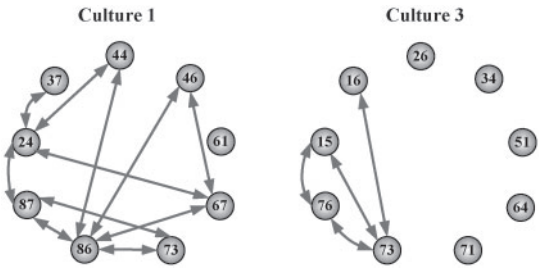

Fig. 4. The maps of identified feedback loops in Cultures 1 and 3. The nodes and their corresponding micro-electrodes were numbered according to their locations on the MEA. The feedback loops were denoted by bi-directional arrows. For Culture 1, 11 feedback loops were found, corresponding to a synchronized oscillatory behavior, while for Culture 3, only 4 feedback loops were found, related to a nearly random behavior

such complexity issues can be alleviated as high-performance computation devices become more available.

In this study, we showed that MSGCM can successfully identify feedback loops in synthetic neural network models and *in vitro* cultured neural networks. We also found that synchronized oscillatory bursting behaviors were closely related to the existence of feedback loops. From this finding, we infer that a feedback loop might be an important network motif for the synchronized oscillatory behavior in pulsed neural networks. In fact, the experiments using *in vitro* cultured neural networks showed that the adjustment of synaptic connections was highly correlated with the development of neuronal network behaviors characterized by the evolvement of spontaneous electrical activities of the network (Muramoto *et al*., 1993; Van Huizen *et al*., 1985). An interesting phenomenon was that the visibility of synchronized bursting behaviors was dependent on the developing phase of the tested *in vitro* neuron cultures. *In vitro* cultured neural networks showed spontaneous and uncorrelated bursting activities in the beginning, but, after about six DIVs, they exhibited abruptly a synchronized bursting activity (Habets *et al*., 1987). Then a question arises as to what triggered such an emergent property in the cultured neural networks? The feedback identification method proposed in this study provides a very useful tool to infer a network motif responsible for this emergent property. Previous studies indicated that developing neurons showed their maximum synchronized activities at the 2nd or 3rd week of the brain development (Habets *et al*., 1987) and after that neuronal circuits reached an optimal connectivity by pruning their connections (Van Huizen *et al*., 1985), i.e. undergoing an overall decline in the number of synapses. We can also find such a development trend by tracing the variation of feedback loop abundance in Table 3 (the number of feedback loops: 11 → 22 → 4 for DIV: 14 → 18 → 21). As the networks are considered to be randomly connected, it would be reasonable to presume that the abundance of feedback loops is positively correlated with the whole network connectivity. Thus, identifying feedback loops using MSGCM can also be validated from this comparison.

Although we showed in this article the identification of feedback loops in cultured neural networks and investigations into the relationship between the structure of a network and its dynamical behavior, the presented approach can also be applied to studying other biological networks based on time-series measurements using, for example, real-time PCR (Heid *et al*., 1996), immunofluorescence (Henle and Henle, 1966) and microarray (Schena *et al*., 1995). If the dynamical response of a biological network can be measured and obtained in the form of multivariate time-series data, MSGCM can be used to investigate the underlying causal feedback connections in the network. For instance, recent advances in neural imaging devices have provided enormous time-course data from the brain. Examples include macroscopic electroencephalography and magnetoencephalography signals recorded from the scalp, invasive electrocorticography from the cortical surface and mesoscopic local field potential with electrodes inserted deep inside the brain. These data have opened a new era for experimental studies on the detailed wiring structure of a functional neural network (He *et al*., 2011). Most of the studies to date, however, have dealt with the functional connectivity of a brain using simple correlation or effective connectivity of a local brain region. MSGCM enables us to construct a functional feedback network covering the whole brain regions and to further project a brain network to a more precise interaction map compared with previous studies. Our method can also be used as a useful tool for examining the functional connectivity anomalies occurring in patients with psychiatric disorders.

Funding: National Research Foundation of Korea (NRF) grants funded by the Korea Government, the Ministry of Education, Science & Technology (MEST) (2009-0086964 and 2010-0017662); The WCU (World Class University) program (R32-2008-000-10218-0) and the Brain Research Center of the 21st Century Frontier Research Program.

Conflict of interest: None declared.

REFERENCES

Alon,U. (2007) Network motifs: theory and experimental approaches. *Nat. Rev. Genet.*, **8**, 450–461.

Baccala,L.A. and Sameshima,K. (1999) *Direct Coherence: A Tool for Exploring Functional Interactions among Brain Structures, Methods for Neural Ensemble Recordings*. CRC press LLC, Boca Raton.

Baccala,L.A. *et al*. (1998) Studying the interaction between brain structures via directed coherence and Granger causality. *Appl. Signal Processing*, **5**, 40.

Brandman,O. *et al*. (2005) Interlinked fast and slow positive feedback loops drive reliable cell decisions. *Science*, **310**, 496–498.

Brillinger,D.R. (2001) *Time Series: Data Analysis and Theory*. SIAM, Society for Industrial Mathematics. Holt, Rinehart. & Winston, New York.

Cadotte,A.J. *et al*. (2008) Causal measures of structure and plasticity in simulated and living neural networks, *PLoS One*, **3**, e3355.

Caines,P. and Chan,C. (1975) Feedback between stationary stochastic processes. *IEEE Trans. Automat. Contr.*, **20**, 498–508.

Chong,S.A. *et al*. (2011) Synaptic dysfunction in hippocampus of transgenic mouse models of Alzheimer's disease: a multi-electrode array study. *Neurobiol. Dis.*, **44**, 284–291.

Dong,C.-Y. *et al*. (2009a) Systematic analysis of synchronized oscillatory neuronal networks reveals an enrichment for coupled direct and indirect feedback motifs. *Bioinformatics*, **25**, 1680–1685.

Dufour,J.M. and Renault,E. (1998) Short run and long run causality in time series: theory. *Econometrica*, **66**, 1099–1125.

Eisen,H. *et al*. (1967) Regulation of repressor inhibition in lambda. *Proc. Natl Acad. Sci. USA*, **66**, 855–862.

Eytan,D. *et al*. (2003) Selective adaptation in networks of cortical neurons. *J. Neurosci.*, **23**, 9349–9356.

Eytan,D. *et al*. (2004) Dopamine-induced dispersion of correlations between action potentials in networks of cortical neurons. *J. Neurophysiol.*, **92**, 1817–1824.

Glendinning,P. (1994) *Stability, Instability and Chaos: An Introduction to the Theory of Nonlinear Differential Equations*. Cambridge University Press, Cambridge.

Golub,G.H. and Van Loan,C.F. (1996) *Matrix Computations*. Johns Hopkins University Press, Baltimore, MD.

Granger,C.W.J. (1969) Investigating causal relations by econometric models and cross-spectral methods. *Econometrica*, **37**, 424–438.

Habets,A. *et al*. (1987) Spontaneous neuronal firing patterns in fetal rat cortical networks during development in vitro: a quantitative analysis. *Exp. Brain Res.*, **69**, 43–52.

Hannan,E.J. and Quinn,B.G. (1979) The determination of the order of an autoregression. *J. Roy. Stat. Soc. Ser. B Methodol.*, **44**, 190–195.

He,B. *et al*. (2011) Electrophysiological imaging of brain activity and connectivity—challenges and opportunities. *IEEE Trans. Biomed. Eng.*, **58**, 1918–1931.

Heid,C.A. *et al*. (1996) Real time quantitative PCR. *Genome Res.*, **6**, 986–994.

Henle,G. and Henle,W. (1966) Immunofluorescence in cells derived from Burkitt's lymphoma. *J. Bacteriol.*, **91**, 1248–1256.

Hill,D.N. *et al*. (2011) Quality metrics to accompany spike sorting of extracellular signals. *J. Neurosci.*, **31**, 8699–8705.

Jimbo,Y. *et al*. (1999) Simultaneous induction of pathway-specific potentiation and depression in networks of cortical neurons. *Biophys. J.*, **76**, 670–678.

Kang,G. *et al*. (2009) Agarose microwell based neuronal micro-circuit arrays on microelectrode arrays for high throughput drug testing. *Lab Chip*, **9**, 3236–3242.

Kashtan,N. *et al*. (2002) *Mfinder Tool Guide*. Weizmann Institute of Science, Rehovot Israel.

Kim,J.R. *et al*. (2008) Coupled feedback loops form dynamic motifs of cellular networks. *Biophys. J.*, **94**, 359.

Lütkepohl,H. (2005) *New Introduction to Multiple Time Series Analysis*. Springer, Berlin.

Maeda,M. *et al*. (2004) Periodic signaling controlled by an oscillatory circuit that includes protein kinases ERK2 and PKA. *Science*, **304**, 875–878.

Marom,S. and Shahaf,G. (2002) Development, learning and memory in large random networks of cortical neurons: lessons beyond anatomy. *Q. Rev. Biophys.*, **35**, 63–87.

Muramoto,K. *et al*. (1993) Frequency of synchronous oscillations of neuronal activity increases during development and is correlated to the number of synapses in cultured cortical neuron networks. *Neurosci. Lett.*, **163**, 163–165.

Porta,A. *et al*. (2002) Quantifying the strength of the linear causal coupling in closed loop interacting cardiovascular variability signals. *Biol. Cybern.*, **86**, 241–251.

Ross,S.M. (1996) *Stochastic Processes*. Wiley, New York.

Ruppert,D. and Wand,M.P. (1994) Multivariate locally weighted least squares regression. *Ann. Stat.*, **22**, 1346–1370.

Sasaki,K. *et al*. (1989) Multiple Purkinje cell recording in rodent cerebellar cortex. *Eur. J. Neurosci.*, **1**, 572–586.

Schena,M. *et al*. (1995) Quantitative monitoring of gene expression patterns with a complementary DNA microarray. *Science*, **270**, 467–470.

Schnider,S.M. *et al*. (1989) Detection of feedback in the central nervous system using system identification techniques. *Biol. Cybern.*, **60**, 203–212.

Schreiber,F. and Schwobbermeyer,H. (2005) MAVisto: a tool for the exploration of network motifs. *Bioinformatics*, **21**, 3572–3574.

Shahaf,G. and Marom,S. (2001) Learning in networks of cortical neurons. *J. Neurosci.*, **21**, 8782.

Strogatz,S.H. (2000) *Nonlinear Dynamics and Chaos: With Applications to Physics, Biology, Chemistry, and Engineering*. Perseus Books Group, New York.

Tiao,G.C. and Box,G.E.P. (1981) Modeling multiple time series with applications. *J. Am. Stat. Assoc.*, **76**, 802–816.

Van Huizen,F. *et al*. (1985) Synaptogenesis in rat cerebral cortex cultures is affected during chronic blockade of spontaneous bioelectric activity by tetradotoxin. *Brain Res.*, **19**, 67–80.

Wernicke,S. and Rasche,F. (2006) FANMOD: a tool for fast network motif detection. *Bioinformatics*, **22**, 1152–1153.

Wolpert,L. and Lewis,J.H. (1975) Towards a theory of development. *Fed. Proc.*, **34**, 14–20.

Wylie,D.R. *et al*. (1995) Temporal relations of the complex spike activity of Purkinje cell pairs in the vestibulocerebellum of rabbits. *J. Neurosci.*, **15**, 2875.